Luminescent Alkylaluminium Anthranilates Reaching Unity Quantum Yield in the Condensed Phase

Vadim Szejko,[a] Iwona Justyniak,*[b] Maria Jędrzejewska,[b] Grzegorz Jędrzejczyk,[a] Thea-Luise Precht,[c] Adam Kubas,[b] Andrew E. H. Wheatley*[c] and Janusz Lewiński*[a,b]

[a] V. Szejko, G. Jędrzejczyk and Prof. J. Lewiński*
Faculty of Chemistry, Warsaw University of Technology, Noakowskiego 3, 00-664 Warsaw, Poland
E-mail: janusz.lewinski@pw.edu.pl

[b] Dr I. Justyniak*, Dr M. Jędrzejewska, Prof. A. Kubas and Prof. J. Lewiński*
Institute of Physical Chemistry, Polish Academy of Sciences, Kasprzaka 44/52,01-224 Warsaw, Poland
E-mail: ijustyniak@ichf.edu.pl

[c] Prof. A. E. H. Wheatley, Dr T.-L. Precht
Yusuf Hamied Department of Chemistry, Cambridge University, Cambridge CB2 1EW, United Kingdom
E-mail: aehw2@cam.ac.uk

Supporting information for this article is given via a link at the end of the document.

Abstract: Transition, post-transition and rare earth metal complexes supported by *(O,N)*- and *(N,N)*-type ligands dominate organometallic photochemistry. However, despite a vast number of aminobenzoate metal complexes having been reported, and aluminium being globally abundant, alkylaluminium anthranilates have not yet been considered as effective luminophores. Herein, using a family of commercially available anthranilic acid (*anth*-H_2) ligands and its *N*-substituted derivatives, we report the isolation and characterisation of a series of unique tetrameric chiral-at-metal alkylaluminium anthranilates, [(R´-*anth*)AlR]$_4$. The resulting compounds are characterised using spectroscopic methods and single-crystal X-ray diffraction to analyze structure-determining factors in the solid state and solution. By then changing the *N*-substituents from H to Me and Ph, we have yielded a series of luminophores that exhibit poor-to-excellent performance, providing a [(Ph-*anth*)AlEt]$_4$ derivative that achieves a unity photoluminescence quantum yield in the condensed phase, which is unprecedented for aluminium complexes.

Introduction

Fluorescent materials based on main-group metal complexes have attracted a lot of interest recently, due to *i.a.* their potential use in optoelectronic devices, a wide range of biological applications or as chemosensors.[1–4] The key advantages of such materials are their ready availability[5] and, unlike many transition metal complexes, low toxicity. The earliest references to luminescent metal complexes can be traced back to the middle of the 19th century.[6] However, 1987 saw a breakthrough, when an Alq_3 (q-H = 8-hydroxyquinoline) compound was presented as the emitting layer in the first light-emitting diode.[7–9] This seminal work provided the impetus for seeking more effective metal complexes with 8-hydroxyquinolinato scaffolds, and in particular, the group 13-based luminescent complexes. Particular attention has been paid to the use of *(O,N)*- and *(N,N)*-bifunctional ligands due to the ease with which their photophysical properties can be tuned (Figure 1).[10–15] Over the last few decades, numerous examples of highly fluorescent Al-based compounds have been reported,[16] *e.g.* *salen* derivatives,[17,18] BODIPY framework-based complexes[19], asymmetric acetylacetonates[20,21] and dinuclear triple-stranded helicates (ALPHY),[22–24] including recently reported dinuclear dimethylaluminium β-diketiminate, $(Me_2Al)_2$BODDI, which exhibited high photoluminescence quantum yield (PLQY) in the condensed phase and solution (Figure 1).[25]

Photoluminescence behaviour is often highly dependent on the aggregate state of the investigated molecular entities. In this context, the effects related to the degree of aggregation, namely aggregation-induced enhancement of emission (AIEE) and aggregation-caused quenching (ACQ), are particularly relevant.[26] The ACQ effect, which is common for most aromatic hydrocarbons and their derivatives, can be explained by intense intermolecular π···π stacking interactions experienced by molecules located in close proximity within the aggregate or cluster. The AIEE process can be mainly understood to operate by mechanisms based on the

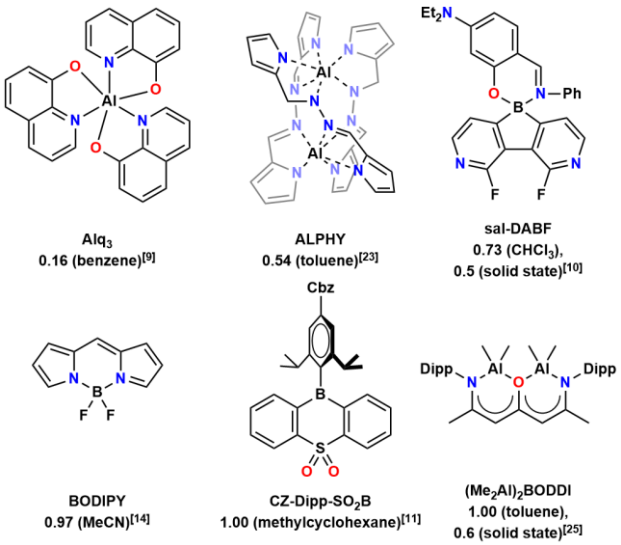

Figure 1. Selected examples of Group 13 luminophores along with their PLQY in solution and in the solid state (if available); Cbz – carbazide group, Dipp = diisoproylphenyl.

restriction of intramolecular rotation.[27] Thus, as molecular packing in the solid plays an important role in determining which of the two effects, AIEE or ACQ, dominate, it is, therefore, important to constantly seek new efficient luminophores in order to gain both a deeper understanding of structure-property relationships and further insights into working mechanisms.[3] Such information will be vital to the systematic design and development of more efficient luminogens.

In recent years, we have manifested a continuing interest in the factors controlling structure [28–33] and reactivity [31–33] of the fertile landscape of organoaluminium carboxylate compounds. A particularly fruitful family constitutes dialkylaluminium complexes of simple carboxylic acids[32] and easy-to-prepare derivatives of phthalic acid[29,33-35] in which one of the two acid groups has been converted to an amino (Figure 2a)[30,31] or other functionality.[28,36,37] These complexes primarily exhibit tetranuclear aggregation, $[(Me_2Al)_2((\mu\text{-}O_2C)C_6H_4\text{-}2\text{-}\mu\text{-}X)]_2$ (X = CO_2^-, NH^- or O^-, respectively), though when the aluminium is sterically hindered, simpler dinuclear aggregates have been reported (Figure 2b,c). It is also noteworthy that a large number of transition, post-transition and rare earth metal complexes derived from quite common aminobenzoic acids have been reported, with a focus on their luminescence properties as driven by their central metal ions.[38] Strikingly, to our knowledge, anthranilates based on non-redox active metal centres have not yet been reported as effective luminophores. Since the use of *(N,N)*- and *(N,O)*-type chelating ligands appears to be beneficial in terms of luminescence properties, we became curious as to whether simple anthranilates could be developed as a ligand of choice in this matter. Herein, we present a series of novel alkylaluminium derivatives of *N*-substituted anthranilic acids, where a unique combination of factors controlling their structure in the solid-state triggers unprecedented luminescent performance of up to unity.

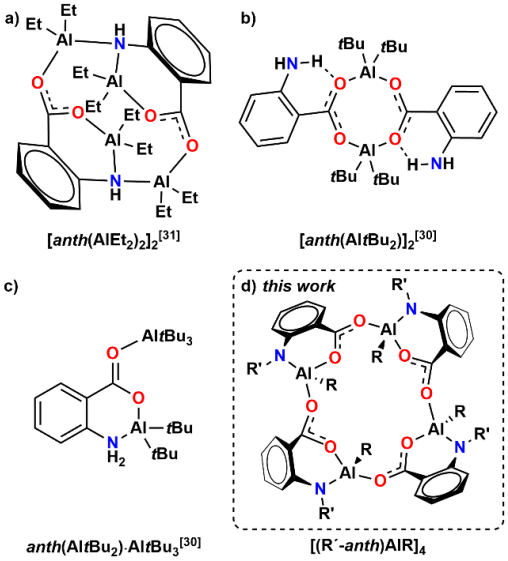

Figure 2. Representation of selected examples of alkylaluminium derivatives of anthranilic acid.

Results and Discussion

In this work, we focus on anthranilic acid (*anth*-H_2) and its *N*-substituted derivatives, methyl (Me-*anth*-H_2) or phenyl (Ph-*anth*-H_2), as model proligands. The reaction between each of these acids and 1 eq. of the appropriate R_3Al compound in toluene has resulted in the formation of a series of aluminium-stereogenic tetranuclear complexes $[(anth)AlMe]_4$ (**1**), $[(Me\text{-}anth)AlEt]_4$ (**2**) and $[(Ph\text{-}anth)AlR]_4$ (where R = Me (**3**) or Et (**4**), Scheme 1) as yellow (for **1** and **2**) or lime-green (for **3** and **4**) crystalline powders in good yield. The resulting compounds are stable solids under an inert atmosphere but slowly decompose in the presence of moisture. They were characterised by elemental analysis, and NMR and FTIR spectroscopies. Single crystals of **1**, **2** and **4** were obtained by recrystallisation from toluene or dichloromethane (DCM), and their identity was further confirmed by X-ray diffraction analysis (SCXRD).

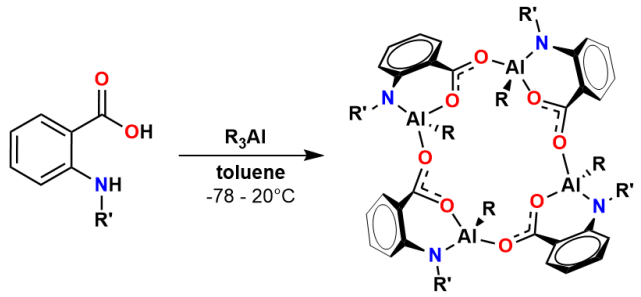

R' = H (*anth*-H_2), Me (*Me-anth*-H_2) or Ph (*Ph-anth*-H_2)

	1	2	3	4
R'	H	Me	Ph	Ph
R	Me	Et	Me	Et
isolated yield, %	21	55	62	58

Scheme 1. Schematic representation of the syntheses of tetranuclear alkylaluminium anthranilates **1**-**4**.

The ^{1}H NMR spectra of freshly dissolved compounds **1-4** confirm double deprotonation of the anthranilic acid (derivatives) in accordance with the stoichiometry of the reaction and include signals from both the alkylaluminium units and the corresponding carboxylate scaffold. Each compound displays two sets of signals indicating the presence of two different entities (for detailed spectroscopic characterisation of compounds **1-4**, see SI). This is exemplified by compound **4** dissolved in C_6D_6 at ambient temperature (hereafter the most extensively studied compound due to its unique photoluminescence properties), where the aliphatic region of ^{1}H spectrum exhibits methyl triplets at 0.95 and 1.27 ppm (assigned **4** and **4´**, respectively, see below) as well as two well-separated resonances for methylene protons; a quartet at 0.40 ppm and what we attribute to a doubled eight-line pattern at -0.14 ppm. The latter multiplet suggests diastereotopic methylene protons, which clearly indicates the chiral nature of the aluminium centres, resulting from aggregation. Interestingly, the spectrum of **4** freshly dissolved in toluene-d_8 at -70°C displays a single set of signals for the $-AlCH_2CH_3$ protons, which allows the explicit identification of the parent tetrameric form (Figure 3). Similarly, the lowfield methylene signal is now absent, and the slightly broadened remaining methylene multiplets are well separated and appear at -0.22 and 0.01 ppm. Upon gradual heating up to 10°C, only a merging of these latter signals is observed and an increase in their intensity along with their slight shift to the high field. Interestingly, at 20°C new multiplet signals evolve which we attribute to a trimeric form **4´** (Figure 3, for a diffusional-ordered experiments, DOSY, *vide infra*). The presence of a quartet for the $-AlCH_2CH_3$ protons of the trimer **4´** indicates the presence of dynamic processes at higher temperatures

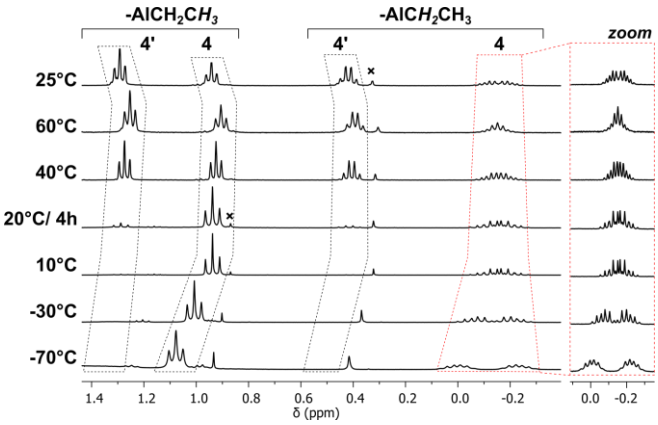

Figure 3. Cropped VT and time-dependent ^{1}H NMR spectra of compound **4** in toluene-d_8; × - impurities. For the complete spectra, see SI, Figure S10.

associated with fast exchange between distinct diastereomers on the NMR timescale.

To gain a more in-depth insight into the character of the anticipated two different aggregates of the [(R´-*anth*)AlR]$_4$ series in solution, DOSY studies were performed for compounds **2**-**4** (for details, see SI). The data confirm that the tetrameric form is retained upon dissolution at lower temperatures. However, after a few hours of storage at ambient temperature, they gradually transform to the trimeric form, reaching a tetramer/trimer ratio *ca.* 2/1. The FTIR spectra of **1**-**4** display essentially identical patterns in the region around 1614-1553 and 1406-1403 cm^{-1}, which is typical for the $\nu_{asym}(CO_2)$ and $\nu_{sym}(CO_2)$ frequencies, respectively, clearly indicating similar coordination of the aluminium centre by the carboxylate group in each case.[39]

The SCXRD analysis confirmed that the molecular forms of **1**, **2,** and **4** are essentially isostructural, but differ in terms of the supramolecular arrangement within the crystal lattice (for the description of supramolecular structures, *vide infra*). Each appears in the solid state as a novel pseudo-centrosymmetric tetranuclear cage with the chiral-at-metal centres adopting a similar CNOO´ coordination environment, which results in the alternate arrangement of monomeric *(R)*- and *(S)*-units. Thus, the configuration of the individual stereogenic centres within the arbitrarily selected molecule can be described as (*R,S,R,S*), which is typical for aggregates seamed from an even number of enantiomers. To our knowledge, the only dimethylaluminium derivative of racemic ethyl lactate monomeric units of the same configuration as the chiral centre in the chelating ligand associate with each other to give a racemic mixture of *(R,R)* and *(S,S)* diastereoisomers, *rac*-[Me$_2$Al{(*S**)-*elac*}]$_2$ (where *elac* = ethyl lactate).[40]

The four R´-*anth* ligands within the macrocycles reported here adopt μ_2-η^2(*N,O*):η^1(*O´*) coordination modes by chelating one Al centre between carboxylic and amino groups and bridging the second Al centre utilizing the remaining carbonyl oxygen atom (Figure 4). The Al-N distances within the series of reported compounds vary in the narrow range of 1.832 – 1.851 Å, depending on the character of the *N*-substituent in the ligand, increasing from H to Ph. The electron density within the carboxylate groups in compounds **1, 2,** and **4** is essentially equally distributed, as evidenced by the nearly equal C-O bond lengths (1.281 – 1.285 Å). The carboxylate group adopts the *syn-anti* conformation commonly found in alkylaluminium derivatives of benzoic acid bearing additional donor *ortho*-functionalities.[28–30] and the Al–O bonds within the 6-membered {AlOC$_3$N} macrocycles formed by the chelating moiety are significantly shorter (1.790 – 1.799 Å) than the bridging Al–O bonds (1.807-1.830 Å).

Complexes **1, 2,** and **4** crystalize in monoclinic *C* 2/c, tetragonal *I*-4, and triclinic *P*-1 space groups, respectively, and significantly differ in their crystal packing. Close inspection of their crystal structures shows the prominent influence of the character of *N*-substituents on the complexes' self-assembly and intermolecular non-covalent interactions. Hershfield surface analysis is useful in the analysis of crystal packing of molecules and interactions between them.[41] This analysis unveils that intermolecular contacts for the title compounds are dominated by H···H contacts that range from 69 to 76%, indicating the significant contribution of van der Waals interactions to their self-assembly (Figures 5 and S24). These weak forces are further affected by more specific intermolecular

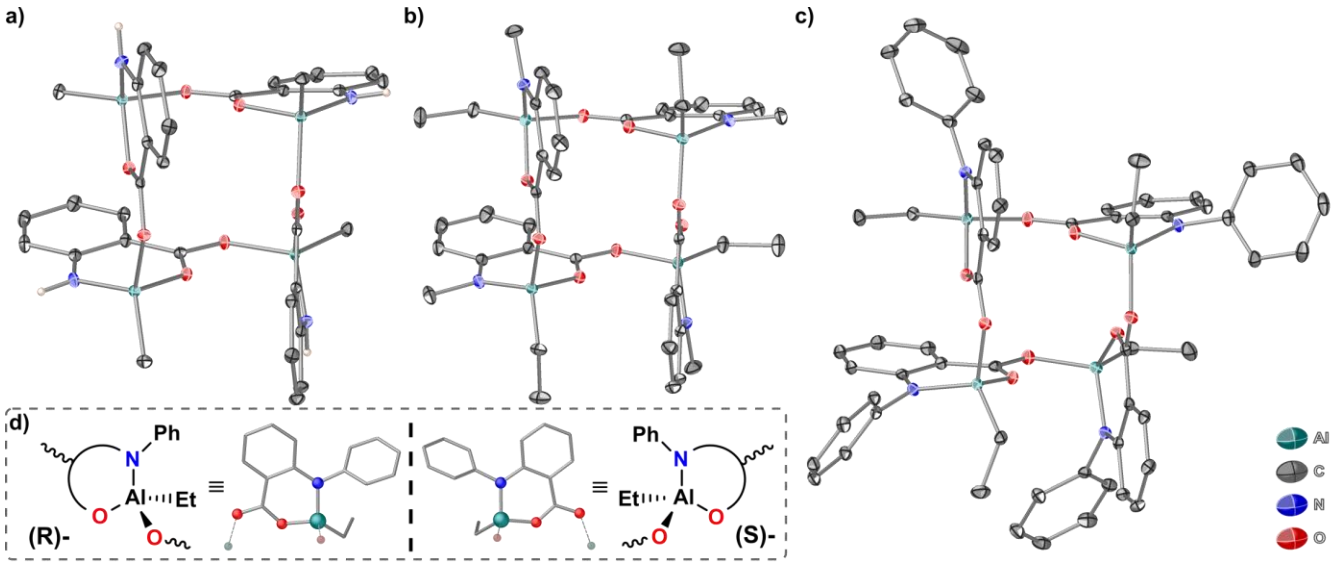

Figure 4. Molecular structures of compounds **1** (a), **2** (b) and **4** (c) with thermal ellipsoids set at 30% probability. d) Stereogenic aluminium centres within compound **4**.C-bonded hydrogen atoms are omitted for clarity.

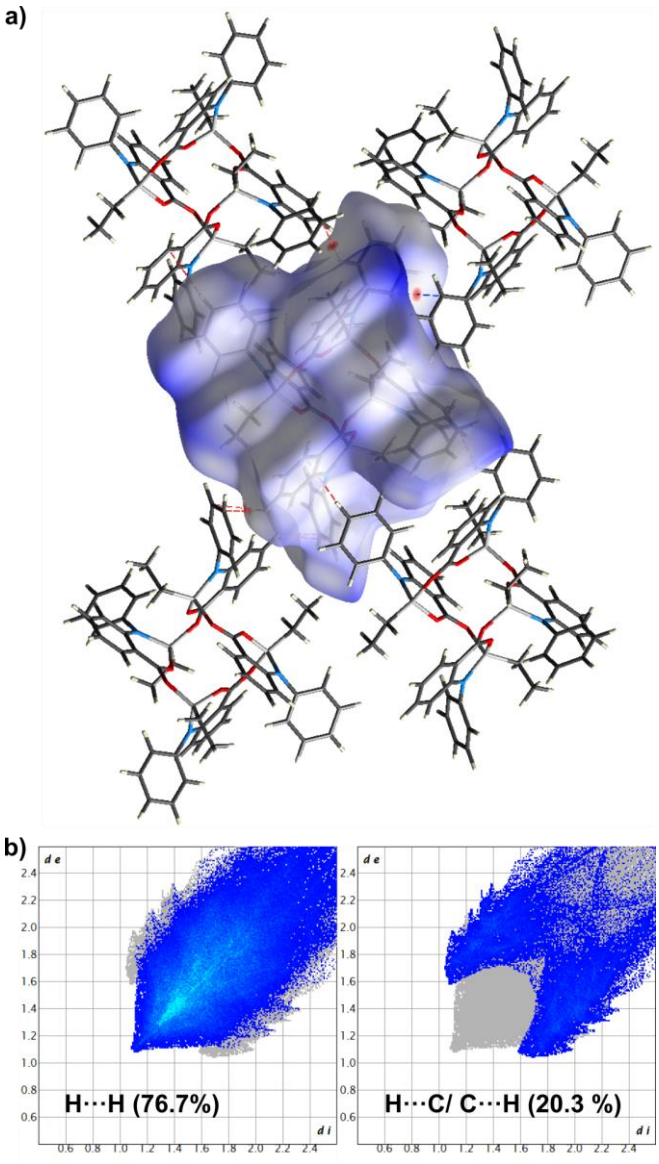

Figure 5. (a) Hirshfeld surfaces (mapped with d_{norm}) and (b) fingerprint plots (d_e vs. d_i) for compound **4**. The colour coding of red, white, and blue spots on the Hirshfeld surfaces indicate the intermolecular contacts with distances less than, equal to, and larger than van der Waals radii, respectively.

interactions depending on the character of the ligand *N*-substituents. For example, the crystal structure of **1** revealed C-H···O interactions involving one of the C_{Ar}-H protons and the oxygen atom of the carboxylate group of a neighbouring molecule (Figure S19). In turn, the supramolecular structure of **2** shows only relatively short intermolecular contacts between carbon atoms of two oppositely arranged carboxylate groups and the peripheral protons of -$AlCH_2CH_3$ of the nearest molecule with the C-H···C distance *ca.* 2.83 Å (Figure S20). The presence of an additional *N*-bonded electron-rich aromatic ring in **4**, results in self-assembly being directed mostly by intermolecular interaction between aromatic moieties, including staggered π···π stacking (parallel displaced) and perpendicular T-shaped C-H···π interactions (Figure S21-23). Notably, these intermolecular interactions are likely to inhibit/restrict ring rotation within the crystal structure of **4**.

The photophysical properties of **1**-**4** in solution and as powders were explored by UV-Vis absorption and photoluminescence (PL) spectroscopy (Figure 6, top) and results are summarised in Table 1. In a dilute degassed toluene solution, all compounds feature a major absorption band at 336-358 nm. Additionally, for **3** and **4**, which both bear *N*-bonded phenyl, an intensive absorption band at 289-290 nm appears. For both alkylaluminium derivatives of *N*-phenylanthranilic acid, the absorption properties do not differ if the alkyl substituent is modified. The influence of solvents such as benzene, DCM and THF was investigated for **4** (Figure S25-26), and it revealed recognisable solvatochromism only in the case of THF as an oxygen donor solvent; the respective DOSY experiment (for details, see Figure S14 and Table S4) indicates that THF does not coordinate to the Al centers but likely solvates the outer-sphere by C-H_{aryl}···O noncovalent interactions. The solid-state spectra of the studied compounds display broad absorption bands in the range from 300 to 450 nm.

To gain insight into the nature of the electronic transitions underlying the absorption bands at the molecular level, time-dependent density functional theory (TDDFT) calculations using the CAM-B3LYP[43] range-separated functional were performed considering the first 40 electronic transitions. The calculated vertical electronic transitions for the anthranilates obtained for the S_0 geometry match well with the experimentally observed photophysical data (Figures 7 and S30). The strong absorption peaks seen in the visible region are calculated to result from intraligand charge transfer (ILCT) transitions, i.e., S_1, S_2, without the contribution

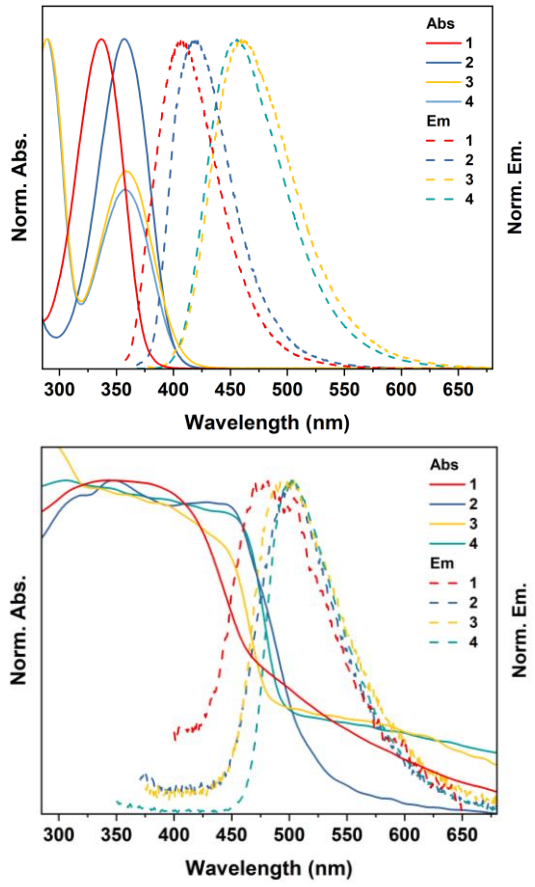

Figure 6. Normalized absorption and emission spectra of compounds **1-4** in degassed toluene solution (top) and in the solid state (bottom).

Table 1. Selected photophysical properties of compounds **1**-**4**.

Compound	λ_{abs} [nm]	λ_{em} (λ_{ex}) [nm]	Stokes shift [cm^{-1}]	Φ_{PL} [a]	τ_{av} [b] [ns]	k_r [c] [10^7 s^{-1}]	k_{nr} [d] [10^7 s^{-1}]
1 (powder)	300-420	469 (300)	2488	0.05	4.3	1.2	22.1
1 (toluene)	336	407 (336)	5192	0.07	-	-	-
2 (powder)	300-450	503 (300)	2342	0.51	8.1	6.3	6.0
2 (toluene)	357	418 (357)	4088	0.62	-	-	-
3 (powder)	350, 450	493 (300)	1938	0.20	3.7	5.4	21.6
3 (toluene)	289, 358	460 (358)	6194	0.26	-	-	-
4 (powder)	300-450	502 (300)	2302	1.00	6.1	16.4	0.0
4 (toluene)	290, 358	455 (358)	5955	0.33	-	-	-

[a] absolute PLQY; [b] average fluorescence lifetime; [c] radiative rate constant, $k_r = \Phi_{PL}/\tau$; [d] non-radiative rate constant, $k_{nr} = (1-\Phi_{PL})/\tau$[42].

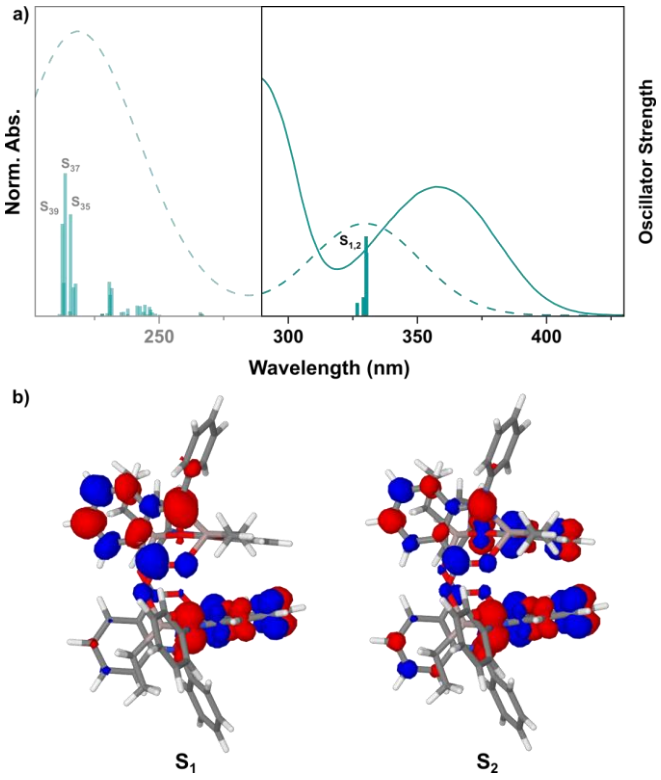

Figure 7. (a) Experimental (solid) and TDDFT calculated (dashed) absorption spectra for **4** in toluene. Electronic transitions (vertical bars) were broadened by Gaussians with a full width at 1/2 maximum of 50 nm. (b) Charge density differences (CDDs) visualizing the nature of prominent electronic transitions S_1 and S_2 (recall Table S10) of **4**; charge transfer occurs from red to blue regions.

of the Al centre. The major contributions ($f_{calc} > 0.4$) are provided by the HOMO−3/−2/−1/0 → LUMO0/+1/+2/+3 transitions. The frontier orbitals are predominantly localized on the *anth* ligand backbone (Figures S29-32) with the HOMO−3/-2/-1/0 dominated by the N *p*-type lone pair, and LUMO0/+1/+2/+3 are mostly localized on the -C_{Ar}COO units. Thus, the absorption process corresponds to the internal π−π* charge transfer from the -N(R´) nitrogen atom to the -C_{Ar}COO unit (Figures 7 and S34-37). The energy of the HOMO orbitals varies slightly with the *N*-substituents (R´ = H, Me, Ph). This observation could be associated with changes in bond polarity around the N-centre, especially in the Al-N bond, as evidenced by Mulliken population analysis. This suggest a substituent-dependent change of the partial nitrogen charge. whilst the Al-O bond polarisation remains essentially unaltered (Table S11).

For all four complexes in degassed toluene at room temperature, intense blue luminescence could be observed following excitation at absorption maximum wavelengths, i.e. 336 nm (for **1**) or 357 nm (for **2**-**4**). As in the UV-Vis absorption spectra, the photoluminescence maxima vary as the ligand is modified (i.e., 407, 418, 460 and 455 nm for **1**, **2**, **3** and **4**, respectively), clearly showing the merits of the ligand modifications in photophysical behaviour (Figure 6, bottom). In toluene, all compounds feature a large Stokes shift, ranging from 4100-6200 cm^{-1}, with almost no overlap between absorption and emission. In the condensed phase,

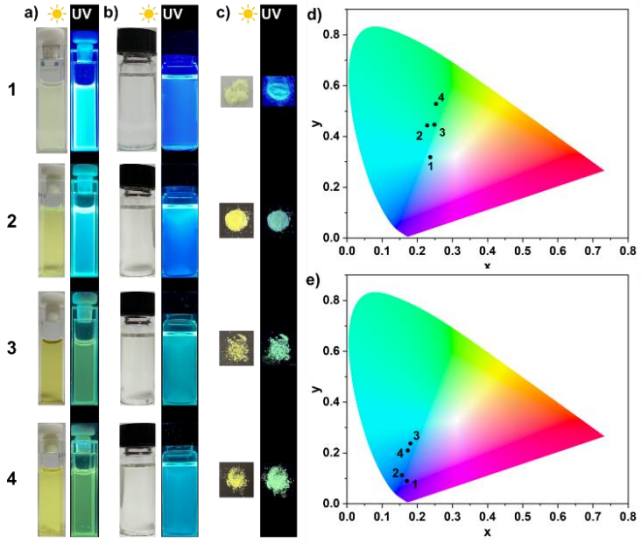

Figure 8. Photographs of **1**-**4** (a and b) as concentrated (ca. 0.7 mg/ml) and diluted toluene solutions (ca. 0.02 mg/ml), respectively; (c) powdered; chromaticity diagrams for (d) powders excited at 300 nm, (e) diluted toluene solutions excited at 360 nm.

following excitation at 300 nm, all compounds exhibit intense photoluminescence, with the bands shifted to 469 - 503 nm, corresponding to green emission (Figure 8). The fluorescence lifetimes of **1**-**4** are in the range of 3.7-8.1 ns (Table 1 and Figure S27), which indicates quantum-mechanically allowed transitions.[44] The emission wavelength in the solid is practically independent of the composition of the compound, which contrasts with the abovementioned emission behaviour in solution. Compounds **1**-**3**, both in the solid state and solution display moderate to high photoluminescence quantum yield (PLQY) (Table 1). Strikingly, in the condensed phase, the ethylaluminium derivative [(Ph-*anth*)AlEt]$_4$ (**4**) demonstrates PLQY around unity, which, to our knowledge, is unprecedented for aluminium complexes. It is worth noting that while the a recently reported dinuclear dimethylaluminium β-oxo-δ-diimine derivative achieved PLQY of 1 in a toluene solution, in the solid PLQY was reduced to 0.5-0.6 (depending whether single-crystal or powdered).[25] Remarkably, fluorescence lifetime values for the investigated anthranilates follow a similar trend to PLQY (Table 1). In the solid state, much faster non-radiative decay for **1** can be rationalized by vibrational quenching, namely high energy vibration of the N–H bond.[45] Replacing H by a Me group (as in **2**) nearly 4-fold reduces the non-radiative constant (k_{nr}), and the remaining quenching can be attributed to the folding of the parent macrocycle as arises from the optimized geometry for the S_1 state of the tetramer (Figure S39). For the methylaluminium derivative **3**, the moderate luminescent performance arises from the speed of non-radiative energy loss through chelate ring fracture. However, when switching to the ethylaluminium derivative **4**, the molecular structure is rigidified by numerous C-H···π interactions which preserve the geometry deformation, resulting in complete blockage of the non-radiative decay pathway (k_{nr} drops to 0 s^{-1}) and opening of the radiative channel. Thus, for **4** the aggregation induces stabilization of the excited states and enhances emission properties.[46]

Conclusion

Inspired by previous observations made using Alq_3, investigations into the effectiveness of luminophores based on main group metal complexes remain ongoing. Aluminium, due to its ubiquity and non-toxicity, in combination with a suitable ligand, seems to be the ideal candidate for a high-performance luminophore. As evidence, a recently published dimethylaluminium β-oxo-δ-diimine derivative achieves the PLQY of 1 in a toluene solution. However, in the solid its efficiency dropped significantly as a consequence of ACQ. We have now presented a series of novel aluminium-stereogenic anthranilates obtained by a simple synthetic procedure using commercially available anthranilic acid and its derivatives. Strikingly, in the solid state, compound **4**, incorporating an anthranilate ligand with a- N bonded phenyl ring, returns a PLQY of 1. To our knowledge, this is the best result to date among Al-based luminophores in the solid state. Overall, the reported results indicate that the observed photophysical processes likely arise from ligand-centred transitions that are facilitated by coordination of the anthranilate ligand to the aluminium centre. Additionally, a particular role for the photophysical performance in the solid state is played by non-covalent interactions that are able to preserve the geometry deformation displayed after excitation and significantly inhibit luminescence-unfavourable relaxation processes. The simplicity of the ligand framework modification offers the possibility of further upgrading of the system to achieve greater chemical stability and enables modulation of the optical properties, which will be important from the point of view of applications.

Supporting Information

The Supporting Information contains experimental details, NMR spectra, X-ray crystallography, UV-Vis/PL measurements computational details, and atomic coordinates for the optimized geometries of the reported compounds. The authors have cited additional references within the Supporting Information.[43,47-65]

Deposition Numbers 2373319 (**1**), 2373320 (**2**) and 2373321 (**4**) contain the supplementary crystallographic data for this paper. These data are provided free of charge by the joint Cambridge Crystallographic Data Centre and Fachinformationszentrum Karlsruhe.

Acknowledgements

The authors acknowledge the financial support of the National Science Centre, Poland (Grant OPUS 19, No. 2020/37/B/ST4/03310; V.S., I.J.). T.-L.P. thanks Schlumberger Cambridge Research Ltd. for funding. Calculations have been carried out using resources provided by Wroclaw Centre for Networking and Supercomputing (https://wcss.pl).

Keywords: luminophore • antranilate ligand • aluminium • chiral-at-metal • quantum yield

[1] J. C. Berrones-Reyes, C. C. Vidyasagar, B. M. Muñoz Flores, V. M. Jiménez-Pérez, *J. Lumin.* **2018**, *195*, 290–313.

[2] B. J. Schwehr, D. Hartnell, M. Massi, M. J. Hackett, *Luminescent Metal Complexes as Emerging Tools for Lipid Imaging*, Springer International Publishing, **2022**.

[3] S. Ito, M. Gon, K. Tanaka, Y. Chujo, *Natl. Sci. Rev.* **2021**, *8*, nwab049.

[4] P. Kaur, K. Singh, *J. Mater. Chem. C* **2019**, *7*, 11361–11405.

[5] C. Bizzarri, E. Spuling, D. M. Knoll, D. Volz, S. Bräse, *Coord. Chem. Rev.* **2018**, *373*, 49–82.

[6] D. C. Freeman, C. E. White, *J. Am. Chem. Soc.* **1956**, *78*, 2678–2682.

[7] C. W. Tang, S. A. Vanslyke, *Appl. Phys. Lett.* **1987**, *51*, 913–915.

[8] D. Z. Garbuzov, V. Bulović, P. E. Burrows, S. R. Forrest, *Chem. Phys. Lett.* **1996**, *249*, 433–437.

[9] S. Katsuta, *Chem. Lett.* **1994**, *23*, 1239–1242.

[10] J. Adamek, P. H. Marek-Urban, K. Woźniak, K. Durka, S. Luliński, *Chem. Sci.* **2023**, *14*, 12133–12142.

[11] M. Urban, P. H. Marek-Urban, K. Durka, S. Luliński, P. Pander, A. P. Monkman, *Angew. Chemie Int. Ed.* **2023**, *62*, e202217530.

[12] R. P. Nandi, P. Chinna Ayya Swamy, P. Dhanalakshmi, S. K. Behera, P. Thilagar, *Inorg. Chem.* **2021**, *60*, 5452–5462.

[13] K. Liu, Z. Jiang, R. A. Lalancette, X. Tang, F. Jäkle, *J. Am. Chem. Soc.* **2022**, *144*, 18908–18917.

[14] X. F. Zhang, J. Zhu, *J. Lumin.* **2019**, *205*, 148–157.

[15] A. Loudet, K. Burgess, *Chem. Rev.* **2007**, *107*, 4891–4932.

[16] S. Wang, *Coord. Chem. Rev.* **2001**, *215*, 79–98.

[17] K. Y. Hwang, H. Kim, Y. S. Lee, M. H. Lee, Y. Do, *Chem. - A Eur. J.* **2009**, *15*, 6478–6487.

[18] K. Y. Hwang, M. H. Lee, H. Jang, Y. Sung, J. S. Lee, S. H. Kim, Y. Do, D.

Transactions, K. Y. Hwang, H. Lee, H. Jang, Y. Sung, S. Lee, H. Kim, *Dalt. Trans.* **2008**, *49*, 1818–1820.
[19] C. Ikeda, S. Ueda, T. Nabeshima, *Chem. Commun.* **2009**, 2544–2546.
[20] K. Nakao, H. Sasabe, Y. Shibuya, A. Matsunaga, K. Katagiri, J. Kido, *Angew. Chemie Int. Ed.* **2021**, *60*, 6036–6041.
[21] K. Hoshi, H. Sasabe, Y. Chiba, N. Yoshida, T. Nakamura, K. Nagasawa, Y. Sayama, H. Katagiri, J. Kido, *Adv. Opt. Mater.* **2024**, 2303303.
[22] T. Ono, K. Ishihama, A. Taema, T. Harada, K. Furusho, M. Hasegawa, Y. Nojima, M. Abe, Y. Hisaeda, *Angew. Chemie Int. Ed.* **2021**, *60*, 2614–2618.
[23] K. Ueno, Y. Konishi, L. Cui, T. Harada, K. Ishibashi, T. Konta, A. Muranaka, Y. Hisaeda, Y. Hoshino, T. Ono, *Inorg. Chem.* **2024**, *63*, 6111–6570.
[24] Y. Konishi, T. Ehara, L. Cui, K. Ueno, Y. Ishigaki, T. Harada, T. Konta, K. Onda, Y. Hoshino, K. Miyata, T. Ono, *Inorg. Chem.* **2024**, *63*, 11716–11725.
[25] F. L. Portwich, Y. Carstensen, A. Dasgupta, S. Kupfer, R. Wyrwa, H. Goerls, C. Eggeling, B. Dietzek, S. Graefe, M. Waechtler, R. Kretschmer, *Angew. Chemie - Int. Ed.* **2022**, *61*, e202117499.
[26] Y. Tang, B. Z. Tang, *Handbook of Aggregation-Induced Emission*, John Wiley & Sons Ltd., **2022**.
[27] J. Mei, N. L. C. Leung, R. T. K. Kwok, J. W. Y. Lam, B. Z. Tang, *Chem. Rev.* **2015**, *115*, 11718–11940.
[28] J. Lewiński, J. Zachara, I. Justyniak, *Organometallics* **1997**, *16*, 3859–3862.
[29] J. Lewiński, J. Zachara, I. Justyniak, *Organometallics* **1998**, *37*, 2575–2577.
[30] C. S. Branch, J. Lewiński, I. Justyniak, S. G. Bott, J. Lipkowski, A. R. Barron, *J. Chem. Soc. Dalt. Trans.* **2001**, *3*, 1253–1258.
[31] J. Lewiński, I. Justyniak, J. Zachara, E. Tratkiewicz, *Organometallics* **2003**, *22*, 4151–4157.
[32] I. Justyniak, D. Prochowicz, A. Tulewicz, W. Bury, P. Goś, J. Lewiński, *Dalt. Trans.* **2017**, *46*, 669–677.
[33] M. Terlecki, I. Justyniak, D. Prochowicz, J. Lewiński, *Eur. J. Inorg. Chem.* **2020**, *2020*, 119–127.
[34] J. Lewiński, W. Bury, I. Justyniak, J. Lipkowski, *Angew. Chemie Int. Ed.* **2006**, *45*, 2872–2875.
[35] W. Ziemkowska, M. Cyrański, A. Kunicki, *Inorg. Chem.* **2009**, *48*, 7006–7008.
[36] C. Redshaw, M. R. J. J. Elsegood, K. E. Holmes, *Angew. Chemie Int. Ed.* **2005**, *44*, 1850–1853.
[37] L. Kalita, R. Pothiraja, V. Saraf, M. G. Walawalkar, R. J. Butcher, R. Murugavel, *J. Organomet. Chem.* **2011**, *696*, 3155–3161.
[38] J. Kalembkiewicz, M. Kosińska, L. Zapała, J. Kalembkiewicz, M. Kosin, *Coord. Chem. Rev.* **2017**, *348*, 25–53.
[39] A. Salifoglou, *Coord. Chem. Rev.* **2002**, *228*, 297–317.
[40] J. Lewiński, J. Zachara, I. Justyniak, *Chem. Commun.* **1997**, *20*, 1519–1520.
[41] P. R. Spackman, M. J. Turner, J. J. McKinnon, S. K. Wolff, D. J. Grimwood, D. Jayatilaka, M. A. Spackman, *J. Appl. Crystallogr.* **2021**, *54*, 1006–1011.
[42] Y. Cui, Y. Yue, G. Qian, B. Chen, *Chem. Rev.* **2012**, *112*, 1126–1162.
[43] T. Yanai, D. P. Tew, N. C. Handy, *Chem. Phys. Lett.* **2004**, *393*, 51–57.
[44] M. Y. Berezin, S. Achilefu, *Chem. Rev.* **2010**, *110*, 2641–2684.
[45] K. Binnemans, *Chem. Rev.* **2009**, *109*, 4283–4374.
[46] Y. Hong, J. W. Y. Lam, B. Z. Tang, *Chem. Soc. Rev.* **2011**, *40*, 5361–5388.
[47] R. Neufeld, D. Stalke, *Chem. Sci.* **2015**, *6*, 3354–3364.
[48] S. Bachmann, B. Gernert, D. Stalke, *Chem. Commun.* **2016**, *52*, 12861–12864.
[49] CrysAlisPro, Data Collection and Processing Software for Agilent Xray Diffractometers, *ver.* 1.171.35.21b, Agilent Technologies, **2012**.
[50] G. M. Sheldrick, *Acta Crystallogr. Sect. C Struct. Chem.* **2015**, *71*, 3–8.
[51] L. J. Bourhis, O. V. Dolomanov, R. J. Gildea, J. A. K. Howard, H. Puschmann, *Acta Crystallogr. Sect. A Found. Crystallogr.* **2015**, *71*, 59–75.
[52] O. V. Dolomanov, L. J. Bourhis, R. J. Gildea, J. A. K. Howard, H. Puschmann, *J. Appl. Crystallogr.* **2009**, *42*, 339–341.
[53] F. Neese, F. Wennmohs, U. Becker, C. Riplinger, *J. Chem. Phys.* **2020**, *152*, 224108.
[54] A. D. Becke, *Phys. Rev. A*, **1988**, *38*, 3098–3100.
[55] F. Weigend, R. Ahlrichs, *Phys. Chem. Chem. Phys.* **2005**, *7*, 3297–3305.
[56] F. Weigend, *Phys. Chem. Chem. Phys.* **2006**, *8*, 1057–1065.
[57] F. Neese, F. Wennmohs, A. Hansen, U. Becker, *Chem. Phys.* **2009**, *356*, 98–109.
[58] S. Grimme, S. Ehrlich, L. Goerigk, *J. Comput. Chem.* **2011**, *32*, 1456–1465.
[59] M. A. L. Marques, E. K. U. Gross, *Annu. Rev. Phys. Chem.* **2004**, *55*, 427–455.
[60] H. Iikura, T. Tsuneda, T. Yanai, K. Hirao, *J. Chem. Phys.* **2001**, *115*, 3540−3544.
[61] J.-D. Chai, M. Head-Gordon, *J. Chem. Phys.* **2008**, *128*, 084106.
[62] M. Casanova-Páez, M. B. Dardis, L. Goerigk, *J.Chem. Theory Comput.* **2019**, *15*, 4735–4744.
[63] A. Hellweg, C. Hattig, S. Hofener, W. Klopper, *Theor. Chem. Acc.* **2007**, *117*, 587–597.
[64] M. Feyereisen, G. Fitzgerald, A. Komornicki, *Chem. Phys. Lett.* **1993**, *208*, 359–363.
[65] A. V. Marenich, C. J. Cramer, D. G. Truhlar, *J. Phys. Chem. B*, **2009**, *113*, 6378–6396.